ADVANCED FUNCTIONAL MATERIALS
www.afm-journal.de

Triboelectric Nanogenerator with Dynamic Electrode for Geological Disaster and Fall-Down Self-Powered Alarm System

Qitao Zhou, Shujun Deng, Along Gao, Boyou Wang, Jianxin Lai, Jing Pan, Lei Huang, Caofeng Pan, Guowen Meng,* and Fan Xia**

Among numerous sensors and alarm systems for the Internet of Things (IoTs), an alarm system for geological disasters or falls directly relates to the safety of people's lives and property. However, the energy supply and complex signal processing limit their wide application and reliability. As an emerging new energy technology, triboelectric nanogenerators (TENGs) can be used as a sensor power supply or even an active self-powered sensor. Unfortunately, for the existing alarm systems based on TENGs, the signal intensity change caused by the occurrence of danger is still limited, making the method of simply judging whether the signal strength exceeds the threshold to alarm not so reliable. Herein, a dynamic electrode for switching high and low output voltage is demonstrated. By introducing short-circuit and air breakdown effects through the novel dynamic electrode, the output voltage of this kind of device in the trigger state is nearly three orders of magnitude higher than that in the normal state. Based on the dynamic electrodes, a series of portable and wearable alarm systems are developed and applied to the fall-down alarm system and rockfall alarm system. Therefore, this work offers a new strategy to improve the reliability of alarm systems for geological disasters or falls and exhibit immense potential in the field of protecting people's lives and property.

1. Introduction

The energy supply problem of the Internet of Things (IoTs) is an important reason that restricts its wider application. Meanwhile, traditional energy storage devices have aggravated the environmental and energy crisis. Therefore, the self-powered sensor systems, which supply power to the sensors in the IoTs by recycling renewable energy in the environment, have attracted more and more attention. Among many renewable energy sources, mechanical energy is the most extensive energy in human and natural environments. At the same time, triboelectric nanogenerator (TENG) has a series of advantages such as low cost, lightweight, high charge density, a wide selection of materials, and flexible structures. Thus, since its invention, TENG has been considered one of the most effective solutions to break through the bottleneck of IoTs' energy supply.[1] Specifically, there are two important branches of research on self-powered systems based on TENG. The requirements for TENGs are different for these two strategies. When working as power supplies,[2] it is particularly important and difficult to ensure the stability of TENGs.[3–7] On the other hand, when TENGs are directly used as active self-powered sensors,[8] accurate capture and analysis of the change of TENG output signals with external stimulation is the key to achieving sensing or alarm.[9] For example, TENGs designed with

Q. Zhou, S. Deng, A. Gao, B. Wang, J. Lai, J. Pan, F. Xia
State Key Laboratory of Biogeology and Environmental Geology
Engineering Research Center of Nano-Geomaterials of the Ministry of Education
Faculty of Materials Science and Chemistry
China University of Geosciences
Wuhan 430074, China
E-mail: xiafan@cug.edu.cn

Q. Zhou, C. Pan
Beijing Institute of Nanoenergy and Nanosystems
Chinese Academy of Sciences
yangyan east rd 8, Beijing 101400, China
E-mail: cfpan@binn.cas.cn

The ORCID identification number(s) for the author(s) of this article can be found under https://doi.org/10.1002/adfm.202306619

DOI: 10.1002/adfm.202306619

L. Huang
Engineering Research Center of Rock-Soil Drilling & Excavation and Protection
Ministry of Education
China University of Geosciences
Wuhan 430074, China

L. Huang
Badong National Observation and Research Station of Geohazards
China University of, Geosciences
Wuhan 430074, China

G. Meng
Key Laboratory of Materials Physics
and Anhui Key Laboratory of Nanomaterials and Nanotechnology
Institute of Solid State Physics
HFIPS
Chinese Academy of Sciences
Hefei 230031, China
E-mail: gwmeng@issp.ac.cn

modularization and encapsulation have been developed to adapt to various harsh environments for mechanical energy harvesting. These TENGs can provide power for various sensors and alarm devices, demonstrating their potential application in emergency self-rescue devices.[10] Meanwhile, active self-powered sensors based on TENG have shown great potential in many fields closely related to human health. For instance, a self-powered sensor based on TENG for landslide displacement and velocity measurements has been successfully demonstrated.[11] Additionally, there is a report on a self-powered multi-point body motion sensing network based on full textile structure, aiming at disease diagnosis and personalized rehabilitation. In order to recognize subtle differences in various motion postures, a machine learning algorithm is employed to assist this system.[12]

Compared with other working principles of alarm systems, it is simpler and more direct to realize sensing or alarm by judging the signal intensity. For example, once the signal intensity exceeds the alarm threshold, the system will directly alarm.[13,14] However, the signal intensity of TENG is easily affected by environmental factors. Actually, the alarm threshold of many TENG alarm systems is equivalent to the intensity of the interference signal, resulting in a high probability of false alarm. The fundamental reason is that the slight stimulus that these systems need to detect or warn is not enough to cause enough signal intensity changes. The false positives are obviously fatal for applications directly related to life safety, such as fall-down alarm systems or geological disaster alarm systems. To resolve this problem, some researchers employed deep learning from artificial intelligence to deeply analyze and mine the characteristics of the signals.[15,16] However, this indirect method is too complex and time-consuming. Actually, there is another solution, which is often ignored due to great difficulty in the implementation. That widens the difference between the alarm threshold and the interference signal, which means that the output signal needs to be enhanced to several orders of magnitude even under small stimulation. Obviously, it is a big challenge to design a universal strategy that can make different types of devices realize the free conversion between ultrahigh output and low output, which is sensitive to the degree of external stimulation.

Herein, a dynamic electrode for switching high and low output voltage has been demonstrated. Based on this dynamic electrode and TENGs, a series of portable and wearable gesture monitoring sensors have been developed. By introducing the short-circuit and air breakdown effects through the novel dynamic electrode, the output voltage of this kind of device in a specific state is nearly three orders of magnitude higher than that in the normal state. In consideration that fall is the most likely reason for old people to obtain traumatic brain injuries,[17] and rockfall or landslides are common and harmful geological disasters,[18] this kind of device is applied to the fall-down alarm system as well as a rockfall warning system and achieved successful detection.

2. Results and Discussion

Figure 1a shows the application of the developed fall-down or rockfall alarm with dynamic electrode structure in the IoTs system to protect personal safety. Figure 1b shows a schematic diagram of the dynamic electrode and the corresponding simplified device. The dynamic electrode is composed of an I-shaped rivet made of Cu, spring, and sponge. The polytetrafluoroethylene (PTFE) ball rolls back and forth between two Cu electrodes, one of them is equipped with the dynamic electrode. Because Cu is more triboelectrically positive than PTFE, electrons will transfer from the Cu electrode to the surface of the PTFE ball. Thus, when they contact with each other, the negative charges will accumulate on the PTFE surface. These triboelectric charges on the PTFE ball are nonmobile and could sustain on the surfaces for a long period of time. When the ball rolls from right to left but does not touch the dynamic electrode, the free electrons of the left Cu electrode cannot flow to the right through the external circuit to neutralize the positive charge. When the ball continues to roll and collide with the dynamic electrode, the I-shaped rivet will contact and get short-circuited with the lower Cu by compressing the sponge. As a result, the free electrons in the left electrode quickly flow to the right electrode. When the ball rolls in the opposite direction, the dynamic electrode and the Cu electrode slowly return to the open circuit state through the rebound of the sponge. Even when the PTFE ball rolls onto the right Cu electrode, the distance between the dynamic electrode and the lower Cu electrode is still very small, resulting in a great electric field between them. Therefore, the breakdown effect occurs, which makes the electrons return and neutralize the positive charge on the left Cu electrode. When the PTFE ball rolls in a small range and does not touch the dynamic electrode, the device works in the single electrode mode and the output voltage is low. Figure S1 and Movie S1, Supporting Information shows the switching of output between high and low voltages as the motion range of the PTFE ball changes.

After demonstrating that the dynamic electrode could realize high and low-voltage switching, it has been extended to other systems to further understand the mechanism and expand its applications. **Figure 2**a shows the smart bracelet with the dynamic electrode as an output performance switching component. Overall, the bracelet consists of a 3D-printed hollow circular tube (two half parts) and electrodes, as well as PTFE balls and a novel dynamic electrode. As a common wearable device, the bracelet has been combined with TENGs. However, most of the current energy harvesting bracelets focus on the combination of dual electromagnetic and TENG to obtain better output performance[19–21] rather than gesture monitoring. By introducing a dynamic electrode, the smart bracelet shown here can switch different output modes under different motion amplitudes.

Figure 2 and Movie S2, Supporting Information show the output performances and corresponding mechanisms of the smart bracelet under different working modes. When the movement amplitude is small, the dynamic part cannot be triggered, only the right electrode is involved in the operation of the device, while the left electrode is an open circuit. Thus, the bracelet can be regarded as working in single-electrode mode (Figure 2b). Specifically, when the PTFE ball slides against the Cu electrodes with surfaces in contact, the positive and negative charges are formed on the Cu electrodes and the PTFE ball surface, respectively. Then, when the PTFE ball slides towards the right-hand electrode (RE), to screen the local field of the nonmobile negative charges on the PTFE ball surface, electrons will flow from the RE to the ground electrode via the load (Figure 2b-ii). When the PTFE ball reaches the overlapping position of the RE, a new balance is achieved (Figure 2b-iii). Subsequently, when the PTFE ball moves

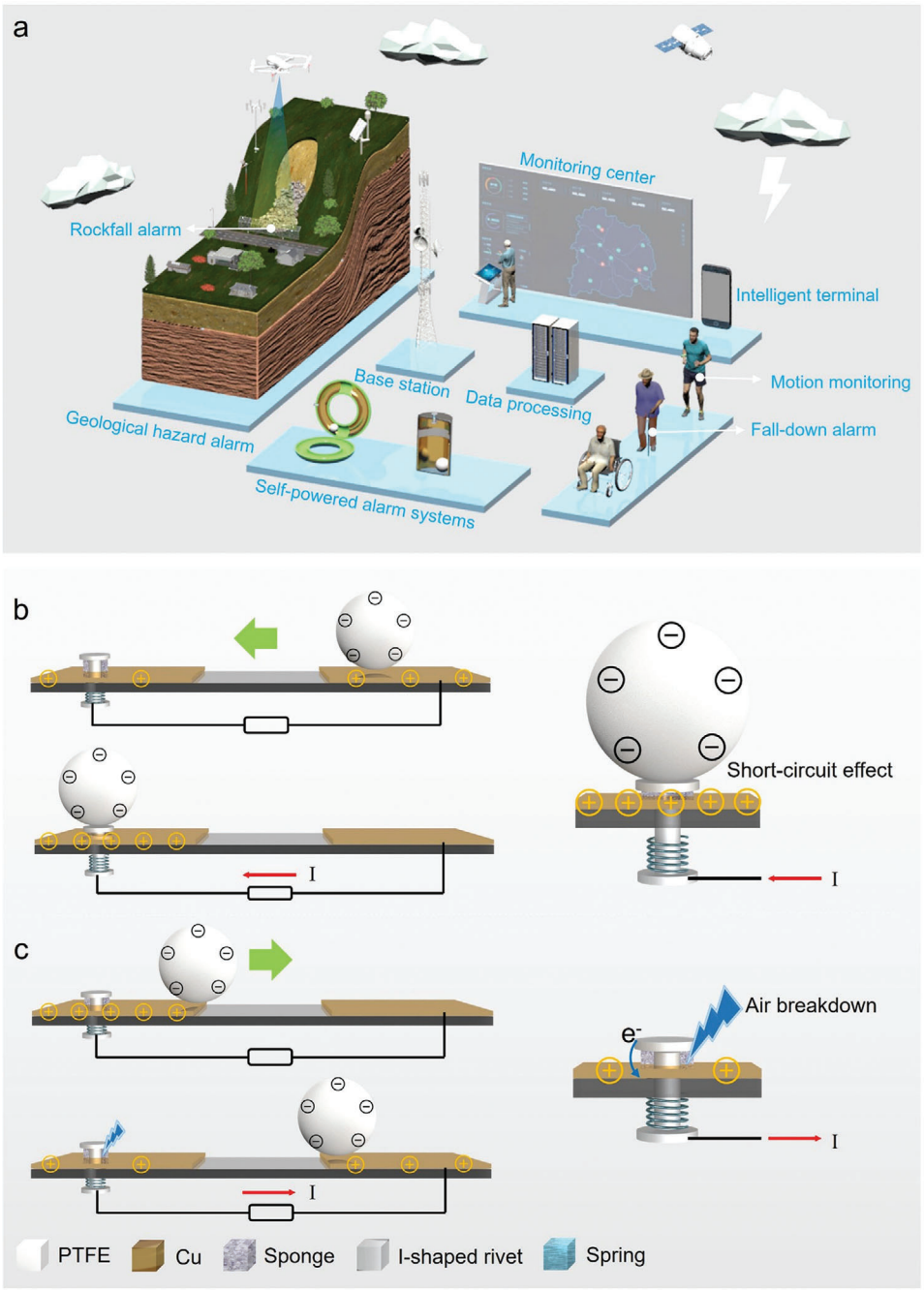

Figure 1. Application scenario and mechanism of the self-powered alarm systems. a) Application scenario of self-powered rockfall alarm system and fall-down alarm system with the high voltage trigger device for personal and property protection. b,c) Schematic diagram of the high voltage trigger device for realizing high voltage output based on short circuit effect and air breakdown effect.

from the RE to the left-hand electrode (LE), electrons are forced to flow in the opposite direction (Figure 2b-iv). In the whole process, the dynamic control device on the left side is not triggered due to the small amplitude of the movement. Therefore, when the ball rolls to the left side, there is no corresponding electrical output. The corresponding output performance is shown in Figure 2b, in which the open-circuit voltage could reach 2.5 V, and the short-circuit current reaches 0.2 μA.

Interestingly, when the amplitude of motion is relatively large, the dynamic part will be triggered, accompanied by a high output signal. As shown in Figure 2c, the open circuit voltage can reach an impressive ≈800 V and the short circuit current can reach about 7 mA. Combined with the schematic (Figure 2c), the reason for the high output can be explained as follows. Similarly, before entering the stable working state shown in the figure, the PTFE ball and the Cu electrode come into physical contact to

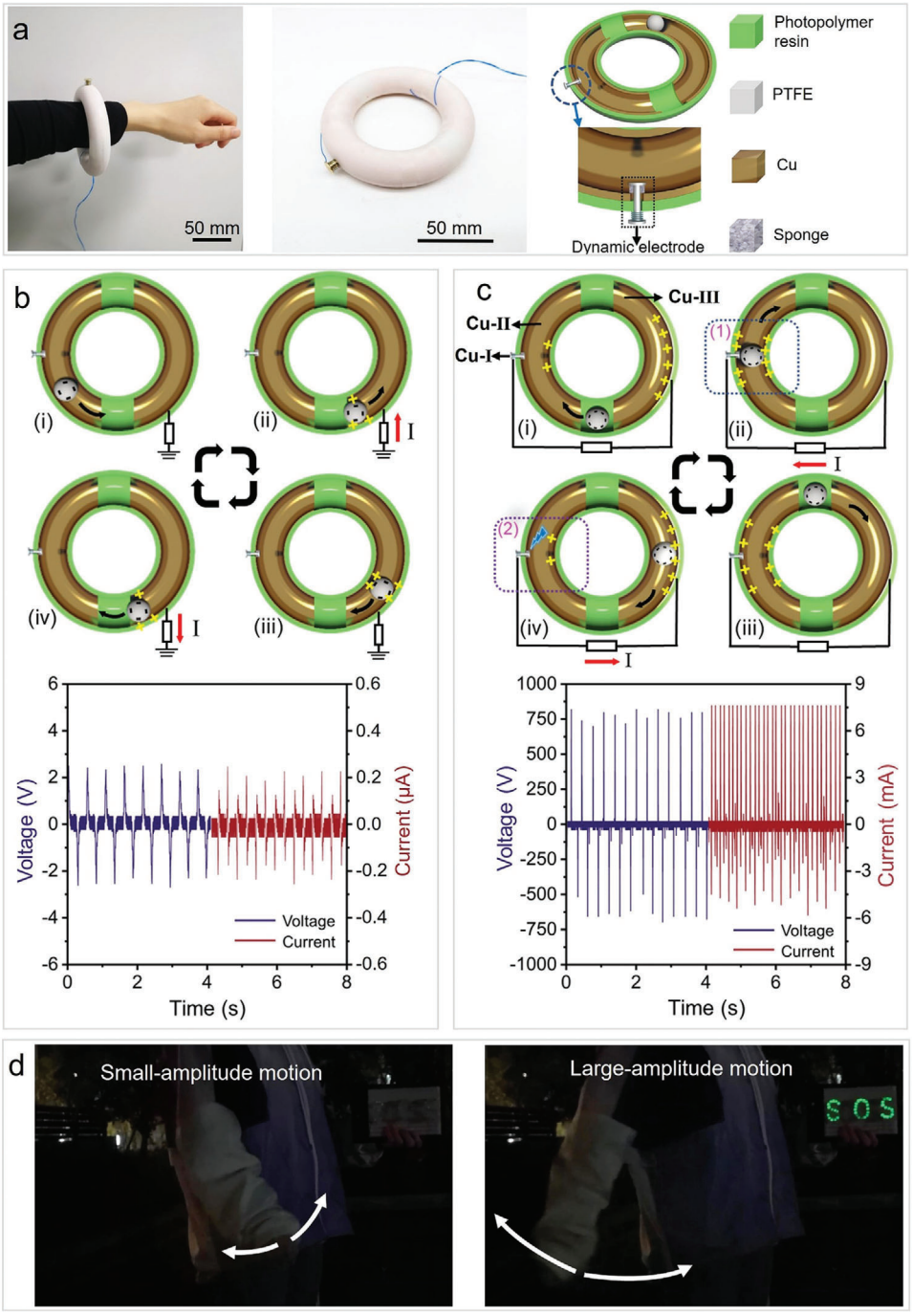

Figure 2. Working mechanism and performance characterization of the smart bracelet with the high voltage trigger element. a) Schematic diagram of the fabricated smart bracelet for energy harvesting and gesture monitoring. b) The working mechanism and corresponding output performance of the smart bracelet when the movement amplitude is small. c) The working mechanism and corresponding output performance of the smart bracelet when the movement amplitude is large. d) Real images of the "SOS" symbol composed of 47 LEDs lightened by increasing the swing range of the arm wearing the smart bracelet.

create triboelectric charges, with the PTEF ball negatively charged and the Cu electrode positively charged according to the triboelectric series. In the stable working state, the electrical signal generation process can be divided into four stages. In stage I, Cu-I (the I-shaped rivet) is apart from Cu electrode Cu-II, they are insulated from each other. Negative charges are preserved on the surface of the PTFE ball and positive charges are distributed in Cu-II and Cu-III. When the PTFE ball rolls over Cu-I, under the pressure of the rolling PTFE ball, Cu-I will contact and get short-circuited with Cu-II by compressing the sponge (stage II).

By establishing a lower potential in Cu-II, the negative charges on the surface of the PTFE ball will induce positive charges in Cu-III to transfer to Cu-II through an external load and Cu-I until the potential difference disappears. After the PTFE ball rolls through the dynamic part, the resilience of the sponge will first make Cu-I separate from Cu-II which will cut off the original circuit to prevent positive charges from flowing back to Cu-III. Thus, when the separation of the PTFE ball from the Cu-II establishes a potential difference again, the positive charges still remain in Cu-II (Figure 2c-iii). This would cause an increase in the electric field intensity between Cu-I and Cu-II, which will induce air breakdown.[22–24] Such breakdown induces an ionized air channel between these two electrodes, allowing the positive charges to transfer back partly to Cu-III, as shown in stage IV. Then the device will restore to the state depicted in stage I.

In order to further prove that the ultra-high output is caused by the dynamic electrode, a bracelet with two symmetrical electrodes without a dynamic part was prepared for comparison. As shown in Figure S2, Supporting Information, the negatively charged PTFE ball rolls inside the hollow tube over the Cu electrodes resulting in the charge flow among two electrodes in order to keep the charge equilibrium state. As shown in Figure S2b, Supporting Information, the open circuit voltage can reach 40 V and the short circuit current can reach about 0.5 μA (Figure S2c, Supporting Information). Although the peak value of the open circuit voltage or short circuit current generated by a smart bracelet with a dynamic electrode is several hundred times higher than that of a two-electrode mode bracelet, there transferred charges are similar (Figure S2d, Supporting Information). This shows that the device with dynamic control device does not increase the amount of transferred charges, but makes the charge transfer more quickly by short circuit and air breakdown effect.

The output performance changes caused by different motion amplitudes can be directly utilized in gesture monitoring. As shown in Figure 2d and Movie S3, Supporting Information, by increasing the swing range of the arm the characters "SOS" consisting of 47 green serially connected LEDs can be lit directly. The distress signal is so clear that it can be clearly identified even outdoors, showing its potential for application in emergency situations. In addition, once this designed system is equipped on life vests, a great deal of expense and time can be saved on inspection and maintenance of power supplies, which is ideal for survival equipment or labor protection equipment that prepare for unpredictable small probability event or outdoor work.

After understanding its working mechanism, the bracelet parameters were discussed more quantitatively. Firstly, the effects of PTFE balls' size on the performance of the smart bracelet have been illustrated. The size of the PTFE balls can significantly affect both the contact area during friction and the speed of contact with the dynamic electrode, thereby impacting the performance of the smart bracelet. Specifically, a comparative experiment was conducted using seven PTFE balls with different diameters (Figure S3, Supporting Information). Considering the diameter of the internal space (20 nm) and the protruding part of the dynamic electrode, the maximum diameter chosen for the PTFE ball was 18 mm, which corresponded to the highest performance of the bracelet in terms of output. However, due to the crowded space, it is challenging to ensure that the PTFE ball (diameter = 18 mm) smoothly passes through the dynamic electrode every time, resulting in non-uniform signals. In contrast, the PTFE ball with a diameter of 16 mm produced a more uniform output signal. However, when the PTFE ball size was reduced to 10 mm or even smaller, the decrease in mass made it difficult to trigger the dynamic electrode. As a result, the output signal became too weak to ensure normal operation and output voltage. Secondly, the spacing between internal Cu electrodes on the performance of the device has been investigated. As shown in Figure S4, Supporting Information, by symmetrically reducing the size of the Cu electrodes, the distance between the Cu electrodes on the left and right sides is increased from 1 to 16 cm. Although the corresponding devices can still function properly, the output voltage is decreased with the increased distance between the Cu electrodes (Figure S4, Supporting Information). This is mainly due to the reduction in the friction-generated charge caused by the reduced surface area of the Cu electrodes. Thirdly, the influence of the number of PTFE balls on the output performance of the bracelet has been studied. With the increase of the number of PTFE balls from 1 to 6, the open circuit voltage is increased from about 800 to 2000 V (**Figure 3**a). Accordingly, the corresponding transferred charge is increased from around 10 to ≈50 nC (Figure S5, Supporting Information). More interesting details can be seen in the enlarged view (Figure 3b). Because the positive pole of the oscilloscope is connected with the I-shaped rivet during the test, the negative voltage signal is caused by the short circuit effect, and the positive voltage signal is caused by the air breakdown effect. In a working cycle, the number of negative voltage peaks increases as the number of balls increases. However, the number of positive voltage peaks did not show a similar change with the increase in the number of PTFE balls. Through the above mechanism explanation, this result can be well explained. The reason why the number of negative voltage peaks increases with the increase in the number of balls is that the negative voltage is caused by the short-circuit effect, and the short-circuit effect only occurs when each ball collides with the trigger part. Thus, the number of negative voltage peaks is consistent with the number of balls. However, the positive voltage signal is caused by the air breakdown effect. That means it is not directly controlled by the number of PTFE balls. The threshold voltage for air breakdown between two parallel plates is described by Paschen's law. [25–27]

$$V_b = \frac{Apd}{ln\,(pd) + B} \tag{1}$$

where V_b is the threshold breakdown voltage, p is the pressure, d is the gap distance between the boards, and A and B are constants related to the gas composition and pressure.

The voltage drop across the air gap V_{air} can be defined as Equation (2).

$$V_{air} = \frac{\sigma S}{C\,(d)} \tag{2}$$

where σ stands for the surface charge density, S is the area of the capacitor plate, and $C(d)$ is the capacitance between two electrodes. For a given d, the V_b can be obtained according to

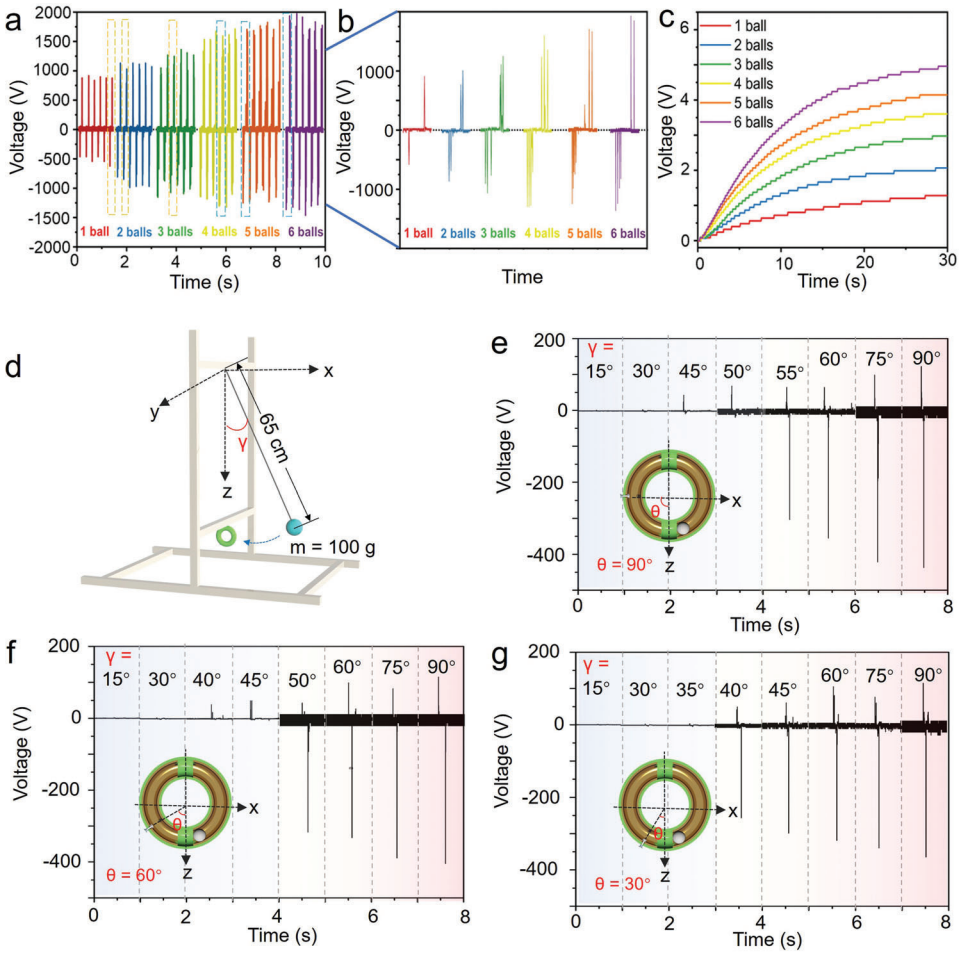

Figure 3. Characterization of the smart bracelet. a) The open circuit voltage of the smart bracelet with the increase of the number of PTFE balls from 1 to 6. b) Enlarged view of the output voltage signals within the dashed box in Figure 3a. c) The measured voltage of a commercial capacitor (1 μF) charged by the smart bracelet with the increase of the number of PTFE balls from 1 to 6. d) Experimental setup for quantitative characterization of high voltage triggering conditions of intelligent ring devices. e–g) The output voltage of the device changes with the swing amplitude of the ball for collision, when the angle between the trigger element and the *z*-axis is 90°, 60°, and 30°, respectively.

Equation (1), and the V_{air} under different surface charge density can be acquired according to Equation (2). Thus, it can be seen that the air breakdown phenomenon occurs only when the surface charge density greater than a critical value σ_d.

Back to the bracelet system, as shown in Figure 2c-iii,iv, when negatively charged PTFE balls are separated from Cu-II one by one and rolled to Cu-III, the surface charge in the equilibrium state is separated again gradually, and the surface charge density of Cu-II will continue to rise until the critical value (σ_d) is reached and air breakdown occurs. The surface charge density decreases rapidly due to air breakdown. Then, when the subsequent PTFE ball continues to roll from Cu-II to Cu-III, the surface charge density continues to accumulate again until the next breakdown occurs. That is to say, not every ball's movement will cause air breakdown. In addition, the charge on each PTFE ball is difficult to be exactly the same, and the time or area of contact with the electrode is also affected by the specific situation. Therefore, the number of positive voltage peaks is relatively random.

Through rectification of the alternating output, the direct output can be stored in energy storage devices such as capacitors. As shown in Figure 3c, the capacitor (1 μF) is charged by the bracelet with different number of PTFE balls. Within 30 s, the capacitor can be charged to 1.2 V by the smart bracelet with one PTFE ball. When the number of PTFE balls increases to 6, the capacitor (1 μF) can be charged to 5 V in 30 s. Meanwhile, the charging status of a series of capacitors with different capacitances by this device is displayed in Figure S6, Supporting Information. As an application, we demonstrated that this bracelet can charge a capacitor (10 μF) and then power an electronic watch. As shown in Figure S7, Supporting Information, in ≈70 s, the voltage of the capacitor reaches around 2.0 V and can later power the watch for more than 10 s. Subsequently, the capacitor can be charged back to 2.0 V in about 40 s and then can power the watch repeatedly. This shows its potential as a power source for electronic devices. At the same time, through the test under different environmental humidity conditions, it can be found that the output voltage of the bracelet can still reach about 360 V even when the relative humidity is as high as 85%. This is a great advantage for the bracelet whether it is used as a power supply or a self-powered sensor (Figure S8, Supporting Information).

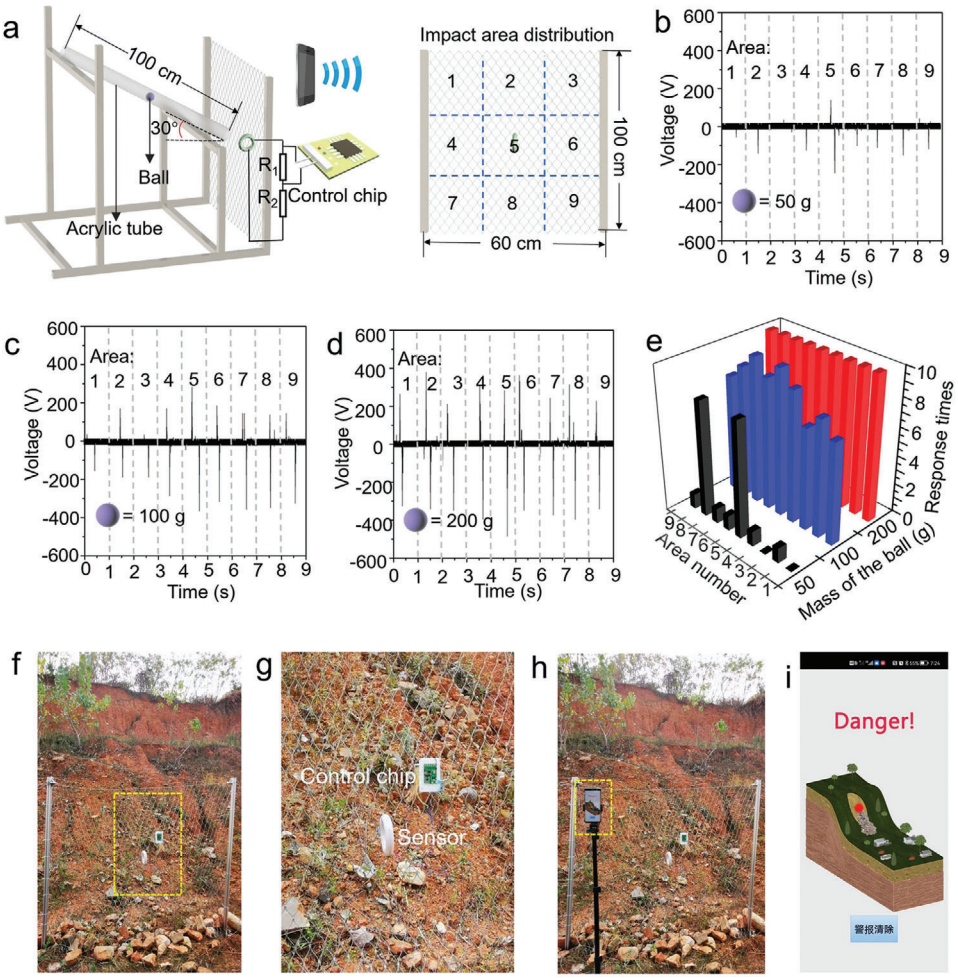

Figure 4. Application of intelligent ring device in self-powered rockfall alarm system. a) Experimental setup for quantitative characterization when the intelligent ring device is used as a self-powered rockfall alarm system. b–d) The output voltage of the self-powered rockfall alarm system changes with the impact area, when the mass of the ball is 50, 100, and 200 g, respectively. e) Statistics of device alarm times for 10 consecutive collision tests of balls with different weights against different areas. f,g) Experimental setup and scenario for the outdoor test of the self-powered rockfall alarm system. h,i) The alarm system sends an alarm to the mobile phone after the stone fence is hit by rolling stones.

In view of the sensitivity of the device to different vibration amplitudes, we plan to apply it to the early warning of geological disasters such as landslides or rockfall. But before that, the triggering conditions of the high voltage signal need to be quantitatively characterized. To this end, we built the test system as shown in Figure 3d and adjusted the kinetic energy of the small ball when it collided with the smart bracelet by controlling the amplitude of the swing of the small ball, so as to obtain the critical condition for triggering the high voltage. As shown in Figure 3e, when the included angle θ between the trigger element and the z-axis is 90°, the small ball needs a large kinetic energy to collide with the trigger element. Therefore, the critical amplitude angle for triggering the high voltage in this case is 55°. Meanwhile, as the judgment basis of trigger, a high negative signal that is almost impossible to be misjudged is generated. As shown in Figure 3f,g, by further adjusting the value of angle θ, the amplitude angle at which the high voltage signal is triggered can be adjusted. For example, when the angle θ is 30°, the critical amplitude angle required for triggering falls to 40°. In other words, the sensitivity of the sensor can be adjusted.

In the above experiment, the small ball as the mechanical energy input directly collides with the device. Obviously, the probability of this situation is very small for real situations such as rockfalls or landslides. Therefore, experiments closer to the real situation were carried out to study the high voltage signal triggering or alarm response when the device was not directly impacted (**Figure 4**a). It can be seen that the net of 0.6 m^2 is evenly divided into nine areas, and the bracelet is located in the center of the net. Then, small balls of different weights are rolled down along the acrylic tube with a fixed length (65 cm) and inclination angle (30°) to impact different areas of the net, and the generated electrical signals are recorded. It can be seen that the signals in areas 5 and 8 are stronger when a small ball with a mass of 50 g is used for impact (Figure 4b). When the mass of the small ball increases, the signal of each area is enhanced. For example, when the mass of the small ball is 200 g, the negative part of the electric signal generated in each impact area exceeds −200 V (Figure 4d).

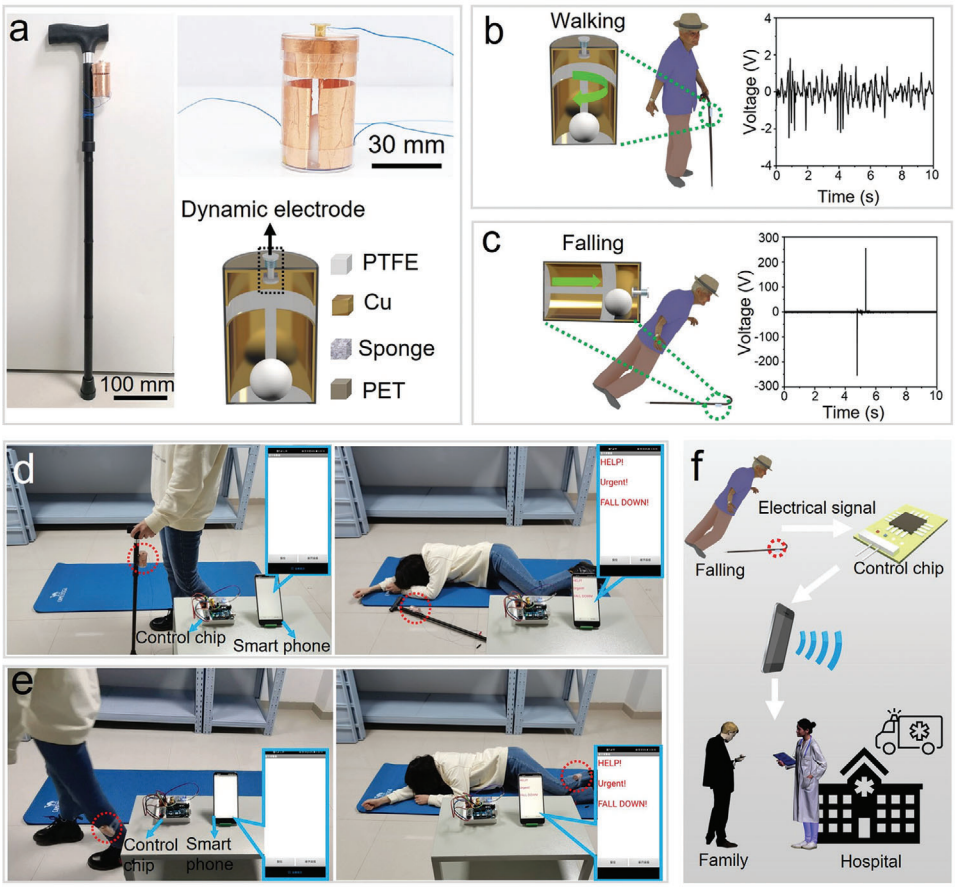

Figure 5. Applications of the fall-down alarm system. a) Schematic diagram of the fall-alert system which is wearable or part of an intelligent crutch. b,c) The output performances of the fall-down alarm system in the case of normal walking and falling. d,e) Application demonstration of the fall-down alarm system combined with a crutch or as a wearable device. f) Illustration of a fall-down alarm system for healthcare monitoring and early warning.

In the above cases, it can be noted that the generated electrical signals exceed the detection range of the voltage of the single-chip microcomputer. Therefore, the simple voltage dividing method as shown in Figure 4a is adopted, so that the voltage detected by the single-chip microcomputer is only a small part of the voltage generated by the bracelet. For example, when R_1 is 60 Ω and R_2 is 4.7 kΩ if the voltage of the single-chip microcomputer alarm is 2 V, the voltage generated by the corresponding bracelet needs to exceed 159 V. The significance of this is that the real environment is very complex, to avoid false alarms, the sensor sensitivity should not be too high. For example, the trigger voltage of 159 V almost eliminates the possibility of false alarms caused by small disturbances. Meanwhile, by simply adjusting the ratio of R_1 and R_2, the trigger voltage provided by the bracelet can be adjusted according to the sensitivity requirements of different application scenarios. At the same time, due to the limited accuracy of the test equipment and the complex interaction of the ball, the net and the bracelet, the reference value of the electric signal given here is limited. Therefore, a more valuable experiment was carried out, that is, each area was repeatedly tested 10 times and the number of times the alarm was triggered was recorded. It can be seen from the figure that when the ball mass is 50 g, the alarm rate is high in only a few areas, which is basically consistent with the trend of electric signal data. Accordingly, when the ball mass is 200 g, all areas can achieve 100% alarm (Figure 4e and Movie S4, Supporting Information).

Then, the performance of the device is verified in a more realistic geological disaster scenario. As shown in Figure 4f,g, the device is fixed on the slope stone fence network to alarm for falling rocks. From Movie S5, Supporting Information, it can be seen that as the falling rocks roll down and hit the stone fence and trigger the sensor, the mobile phone will soon receive the corresponding alarm signal (Figure 4h,i). What is more, the system can give an alarm for small or large stones, whether they collide with the net or the crossbar of the fixed net. This greatly guarantees the reliability of the system.

Then, in order to verify the universality of the high voltage signal triggering principle, a fall-down alarm system for elderly people has been developed (**Figure 5**a). The delay of immediately informing the relatives or hospital staff after tripping is the main reason for further complications, and possibly death caused by fall.[28] Therefore, a portable self-powered real-time fall-down alarm system based on TENG was demonstrated to respond to this issue. Figure 5b,c shows the output performance of the fall detector in case of normal walking and falling. When walking normally, the output voltage is about 2 V,

while when falling, it can produce a voltage higher than 200 V. The signal strength is enhanced by nearly two orders of magnitude. However, in the existing devices, the difference is only a few times, or the waveform of the signal needs to be deeply analyzed.[29]

The corresponding mechanisms of the fall-alert microsystem in different working modes have been shown in Figure S9, Supporting Information. The PTFE ball and the electrodes are uncharged at first, static charges are then introduced by the triboelectrification effect when they are in physical contact. As shown in Figure S9a, Supporting Information, the PTFE ball rotates at the bottom of the TENG, while normal walking and only the bottom electrodes (BEs) Cu-I and Cu-II are involved in the operation of the device. Specifically, when the PTFE ball slides against the Cu electrodes with surfaces in contact, the triboelectric effect will make the PTFE surface with negative charges, and the Cu-I electrode with positive charges (Figure S9a-i, Supporting Information). Meanwhile, a potential difference will be constructed between Cu-I and Cu-II electrodes. Then, when the PTFE ball slides away from the Cu-I electrode to the Cu-II electrode, the positive charges will flow from the Cu-I to the Cu-II via the load to keep the electrostatic balance (Figure S9a-ii, Supporting Information), until the PTFE ball is in full contact with Cu-II electrode (Figure S9a-iii, Supporting Information). Then, a backward sliding of the PTFE ball from the Cu-II electrode to the Cu-I electrode should drive the flow of the positive charges from the Cu-II to Cu-I, forming a reverse current in the load (Figure S9a-iv, Supporting Information). The corresponding output performance is shown in Figure S9b, Supporting Information, in which the open-circuit voltage could reach 3.8 V, and the short-circuit current reaches 0.1 μA.

Figure S9c,d, Supporting Information shows the corresponding mechanisms and electrical performance of the fall detector in case of falling. The working mechanism of high output is similar to the bracelet. Combined with the schematic (Figure S9c, Supporting Information), the mechanism is explained as follows. Similarly, before entering the stable working state shown in the figure, the PTFE ball and the Cu electrode contact to generate triboelectric charges, with the PTFE ball negatively charged and the Cu electrode positively charged according to the triboelectric series. When walking normally, the Cu-IV is apart from the Cu-III electrode, and negative charges are preserved on the surface of the PTFE ball and positive charges distribute in the Cu electrode at the bottom (Cu-I and Cu-II) of the TENG (stages I and II). When falling, Cu-IV will contact with the PTFE ball, then get short-circuited with Cu-III by compressing the sponge. By creating a lower potential in Cu-III, the negative charges on the surface of the PTFE ball will induce positive charges in BE to transfer to Cu-III through an external load and Cu-IV until the potential difference disappears (stage III). When the ball moves back and is no longer in contact with Cu-IV, the resilience of the sponge will first make Cu-IV separate from Cu-III as will cut off the original circuit to prevent positive charges from flowing back to BE. Thus, when the separation of the PTFE ball from Cu-III establishes a potential difference again, the positive charges still remain in Cu-III. This would cause an increase in the electric field intensity between Cu-III and Cu-IV in further separation, which will induce air breakdown. Such breakdown induces an ionized air channel between these two electrodes, allowing the positive charges to transfer back partly to BE (stage IV). Then the device will restore to the state depicted in stage I. Similarly, by controlling the device with a hand to simulate the process of falling, it can be seen that the corresponding output performance open-circuit voltage could reach around 400 V, and the short circuit current reaches around 3 mA (Figure S9d, Supporting Information). More importantly, this high output signal can only be triggered when the device is turned over 90°, which greatly reduces the possibility of false touch. By controlling the device with a hand to simulate the process of walking and falling, it can be seen that the repeatability of the device is very good (Movie S6, Supporting Information).

At last, a relatively complete fall-down alarm system has been demonstrated. As shown in Figure 5d,e, the alert system includes three parts: i) Monitoring the movement state: TENG with dynamic electrode serves as a fall detector to generate a high voltage signal when someone falls down; ii) signal process and communication: a microprocessor with a Bluetooth module was used to receive and process electrical signals and send information; iii) remote terminal, such as cellphone or other portable electronics, to receive the emergency message of falling down (Movies S7 and S8, Supporting Information). Through the general network and intelligent terminal, family members and hospitals were informed promptly when the wearer fell (Figure 5f). The system is expected to be widely applied in online monitoring and home health care.

3. Conclusion

Here, we showed a dynamic electrode that can make the output voltage of the TENG switch freely between high and low voltages. Then, we demonstrated a TENG-based smart bracelet, rockfall alarm system, and intelligent crutch with dynamic electrodes. Under normal conditions, they can be used to recover the mechanical energy generated by human movement to power electronic manufacturing. Meanwhile, in the case of large movement, the short-circuit effect and air breakdown effect caused by triggering the dynamic electrode produce signals several orders of magnitude higher than usual. Therefore, these devices can be used as gesture monitoring, rockfall alarms, or fall-down alarm systems. All of the above show its remarkable potential for geological disasters or fall-down alarm applications in a reliable, simple, convenient, and inexpensive manner.

4. Experimental Section

Fabrication of the Smart Bracelet: A hollow bracelet (two half parts, 20 mm inner diameter and 1.5 mm thickness) was fabricated by using a 3D printer (Form 3, Formlabs) with photoinduced polymeric resin as the material. The diameter of the middle part of the bracelet was set to 65 mm. A small round hole (5 mm in diameter) was reserved on the outer wall of the bracelet for installing the dynamic electrode device. Two copper films (60 μm thickness) were pasted on both sides of the inner wall of the bracelet as the electrode and the friction layer. The distance between the two copper films was about 1 cm, and the round hole was in the middle of the copper film on one side. In order to prepare the dynamic electrode, the I-shaped rivet was installed in the round hole. Two ends of the rivet were respectively inside and outside the hollow bracelet. The inner part was

separated from the copper film by a sponge, and the outer part was separated from the shell of the bracelet by a spring. The bracelet was sealed, after putting the PTFE ball into it. Seven different diameters (18, 16, 15, 12.7, 10, 8, and 5 mm) of PTFE balls were selected for testing. The distance between the left and right Cu electrodes in the bracelet was tested by gradually adjusting from 1 to 16 cm. All the parts and materials are clearly illustrated in Figure 2.

Fabrication of the Fall-Down Alarm System: The polyethylene terephthalate (PET) soft plate (0.5 mm thickness) and the upper and lower cover were used as materials to make a hollow cylinder (3.5 cm inner diameter and 6 cm height). Three pieces of copper films were pasted inside the hollow cylinder as triboelectric materials and electrodes. Two of them were symmetrically distributed on the inner wall of the cylinder, and the other one was located on the inner surface of the top cover (Figure S9, Supporting Information). The dynamic electrode was placed on the top cover. A PTFE ball (22 mm in diameter) was placed into the cylinder before encapsulation. All the parts and materials are clearly illustrated in Figure S9, Supporting Information.

Characterization: The open-circuit voltage of the TENG was measured using a digital phosphor oscilloscope (MSO 2024B, Tektronix, Inc., Beaverton, OR, USA) and the electrical measurements were measured using a low-noise current preamplifier (model no. SR570, Stanford Research Systems, Inc., Sunnyvale, CA). The charge transfer from the output signals was measured using an electrometer (Keithley 6514, Cleveland, OH, USA). A Bluetooth module (HC-06, HC-IT, China) was used for the fall warning systems.

Supporting Information

Supporting Information is available from the Wiley Online Library or from the author.

Acknowledgements

This work was supported by the National Natural Science Foundation of China (22004112, 22090050, 51902296, 52125205, U20A20166, 61805015, and 61804011), the National Key R & D Program of China (2021YFA1200403, 2018YFE0206900), the Joint NSFC-ISF Research Grant Program (Grant No: 22161142020), and Zhejiang Provincial Natural Science Foundation of China under Grant No. LD21B050001. In this work, S.D. participated in the completion of the demonstration of the difference in output signals under different magnitudes of the smart bracelet and the fall-down alarm system. A.G. and J.L. completed the indoor testing of the smart bracelet for the self-powered rockfall alarm system. A.G. and B.W. completed the outdoor testing of the smart bracelet for the application of the self-powered rockfall alarm system. Informed signed consents have been obtained from all volunteers for the aforementioned experiments.

Conflict of Interest

The authors declare no conflict of interest.

Data Availability Statement

The data that support the findings of this study are available from the corresponding author upon reasonable request.

Keywords

air breakdown, dynamic electrodes, fall alarm, short-circuit effect, triboelectric nanogenerator

Received: June 12, 2023
Revised: August 2, 2023
Published online:

[1] R. Liu, Z. L. Wang, K. Fukuda, T. Someya, *Nat. Rev. Mater.* **2022**, *7*, 870.
[2] Y. Song, J. Min, Y. Yu, H. Wang, Y. Yang, H. Zhang, W. Gao, *Sci. Adv.* **2020**, *6*, aay9842.
[3] Q. Zhou, K. Lee, K. N. Kim, J. G. Park, J. Pan, J. Bae, J. M. Baik, T. Kim, *Nano Energy* **2019**, *57*, 903.
[4] J. H. Lee, R. Hinchet, S. K. Kim, S. Kim, S.-W. Kim, *Energy Environ. Sci.* **2015**, *8*, 3605.
[5] K. Parida, V. Kumar, W. Jiangxin, V. Bhavanasi, R. Bendi, P. S. Lee, *Adv. Mater.* **2017**, *29*, 1702181.
[6] Z. Qian, R. Li, J. Guo, Z. Wang, X. Li, C. Li, N. Zhao, J. Xu, *Nano Energy* **2019**, *64*, 103900.
[7] A. Chandrasekhar, V. Vivekananthan, G. Khandelwal, S. J. Kim, *Nano Energy* **2019**, *60*, 850.
[8] Q. Zhou, J. Pan, S. Deng, F. Xia, T. Kim, *Adv. Mater.* **2021**, *33*, 2008276.
[9] C. Wu, W. Ding, R. Liu, J. Wang, A. C. Wang, J. Wang, S. Li, Y. Zi, Z. L. Wang, *Mater. Today* **2018**, *21*, 216.
[10] H. Li, Y. Zhang, Z. Gao, L. Liang, X. Wang, X. Liu, Y. Wu, H. Zheng, *Nano Energy* **2023**, *109*, 108266.
[11] Y. Zhang, C. Wu, *IEEE Sens. J.* **2023**, *23*, 18042.
[12] C. Wei, R. Cheng, C. Ning, X. Wei, X. Peng, T. Lv, F. Sheng, K. Dong, Z. L. Wang, *Adv. Funct. Mater.* **2023**, *33*, 2303562.
[13] S. Li, D. Liu, Z. Zhao, L. Zhou, X. Yin, X. Li, Y. Gao, C. Zhang, Q. Zhang, J. Wang, Z. L. Wang, *ACS Nano* **2020**, *14*, 2475.
[14] J. Lai, Y. Ke, Z. Cao, W. Xu, J. Pan, Y. Dong, Q. Zhou, G. Meng, C. Pan, F. Xia, *Nano Today* **2022**, *43*, 101437.
[15] F. Wen, Z. Zhang, T. He, C. Lee, *Nat. Commun.* **2021**, *12*, 5378.
[16] Y. Zhou, M. Shen, X. Cui, Y. Shao, L. Li, Y. Zhang, *Nano Energy* **2021**, *84*, 105887.
[17] N. Thakur, C. Y. Han, *J. Sens. Actuator Networks* **2021**, *10*, 39.
[18] X. Fan, G. Scaringi, O. Korup, A. J. West, C. J. Westen, H. Tanyas, N. Hovius, T. C. Hales, R. W. Jibson, K. E. Allstadt, L. Zhang, S. G. Evans, C. Xu, G. Li, X. Pei, Q. Xu, R. Huang, *Rev. Geophys.* **2019**, *57*, 421.
[19] S. L. Zhang, Q. Jiang, Z. Wu, W. Ding, L. Zhang, H. N. Alshareef, Z. L. Wang, *Adv. Energy Mater.* **2019**, *9*, 1900152.
[20] P. Maharjan, H. Cho, M. S. Rasel, M. Salauddin, J. Y. Park, *Nano Energy* **2018**, *53*, 213.
[21] P. Maharjan, R. M. Toyabur, J. Y. Park, *Nano Energy* **2018**, *46*, 383.
[22] W. He, W. Liu, J. Chen, Z. Wang, Y. Liu, X. Pu, H. Yang, Q. Tang, H. Yang, H. Guo, C. Hu, *Nat. Commun.* **2020**, *11*, 4277.
[23] D. Liu, X. Yin, H. Guo, L. Zhou, X. Li, C. Zhang, J. Wang, Z. L. Wang, *Sci. Adv.* **2019**, *5*, aav6437.
[24] J. Luo, L. Xu, W. Tang, T. Jiang, F. R. Fan, Y. Pang, L. Chen, Y. Zhang, Z. L. Wang, *Adv. Energy Mater.* **2018**, *8*, 1800889.
[25] Y. Zi, C. Wu, W. Ding, Z. L. Wang, *Adv. Funct. Mater.* **2017**, *27*, 1700049.
[26] Z. Su, M. Han, X. Cheng, H. Chen, X. Chen, H. Zhang, *Adv. Funct. Mater.* **2016**, *26*, 5524.
[27] C. Jiang, K. Dai, F. Yi, Y. Han, X. Wang, Z. You, *Nano Energy* **2018**, *53*, 706.
[28] A. L. Silva de Lima, T. Smits, S. K. Darweesh, G. Valenti, M. Milosevic, M. Pijl, H. Baldus, N. M. de Vries, M. J. Meinders, B. R. Bloem, *Mov. Disord.* **2020**, *35*, 109.
[29] R. Li, X. Wei, J. Xu, J. Chen, B. Li, Z. Wu, Z. L. Wang, *Micromachines* **2021**, *12*, 352.